

Measurement of scaling laws for shock waves in thermal nonlocal media

N. Ghofraniha^{1*}, L. Santamaria Amato², V. Folli², S. Trillo³, E. DelRe^{4,1}, and C. Conti^{4,2}

¹IPCF-CNR, UOS Roma Kerberos, Università La Sapienza, P. le A. Moro 2, I-00185, Roma, Italy

²ISC-CNR, UOS Sapienza, P. A. Moro 2, 00185 - Roma, Italy

³Dipartimento di Ingegneria, Università di Ferrara, Via Saragat 1, 44100 Ferrara, Italy

⁴Dipartimento di Fisica - Università La Sapienza, P. A. Moro 2, 00185 - Roma, Italy

*Corresponding author: neda.ghofraniha@roma1.infn.it

Compiled March 3, 2013

We are able to detect the details of spatial optical collisionless wave-breaking through the high aperture imaging of a beam suffering shock in a fluorescent nonlinear nonlocal thermal medium. This allows us to directly measure how nonlocality and nonlinearity affect the point of shock formation and compare results with numerical simulations. © 2013 Optical Society of America

OCIS codes: 000.0000, 999.9999.

Shock waves (SW) are characterized by an abrupt wave-profile, corresponding to discontinuous solutions of hyperbolic partial differential equations [1]. *Dissipative* SW display a smooth wave front, due to viscous damping, whereas *dispersive*, or collisionless, SW exhibit a characteristic oscillatory front. The latter are expected in Hamiltonian universal models for nonlinear media, such as the nonlinear Schrödinger (NLS) equation, in the weakly dispersive regime where hydrodynamical approximations hold true [2–4]. Dispersion regularizes the shock, determining the onset of oscillations that appear near the wavebreaking point, and expand from there [2], as investigated in ion-acoustic waves [5], in fibers [6, 7], in diffracting optical beams [8] or in Bose-Einstein condensates [9]. Nonlocal phenomena [10–14] substantially alter dispersive SW [15–17]. For propagation in highly nonlocal, strongly defocusing, thermal media, previous work has been based on approximating the 3D dimensional Fourier equation for the temperature profile by a nonlocal nonlinearity with a finite degree of nonlocality [16–18].

In this Letter we report on the quantitative investigation of the formation of dispersive shocks from standard laser beams (Gaussian TEM₀₀) in thermal media. The key to our experiments is the direct observation of the intensity profile of the shock wave in its formation and evolution through the use of a fluorescent medium and a high aperture microscope. We quantify the shock position along propagation and show how it depends on nonlinearity and nonlocality. Our results not only confirm the finite degree of nonlocality of thermal media but actually provide a strategy for its direct measurement.

In experiments we use aqueous solutions of RhodamineB (RhB) displaying a thermal defocusing effect due to light absorption. A continuous-wave solid state laser at wavelength $\lambda=532$ nm is focused on the input facet of the sample at the beam radius waist w_0 . We work at two different w_0 (18 μm and 25 μm) to change both nonlinearity and nonlocality and two different RhB concentrations (0.1 mM, sample A; 0.067 mM,

sample B) that vary the nonlinearity. For the visualization of light along its propagation, samples are put in 1cm×1cm×3cm glass cells (propagation along 1cm), and top images are collected through a microscope and recorded by a 1024×1392 pixel CCD camera. Conversely, to detect light transmitted at the exit of the samples, we use 1mm×1cm×3cm glass cells with propagation along the 1mm vertical direction (parallel to gravity) so as to moderate the effect of heat convection. Transverse images of the beam intensity distributions at the exit facet of the cell are collected through a lens and recorded by the CCD camera. Images from the two experimental configurations are reproduced with comparable length-scale.

Numerical simulations are also performed to verify the experimental measurements and to clarify the role of nonlocality. By using a split-step beam propagation method, we numerically integrate the following nonlocal NLS equation (details in [16, 17]):

$$i\frac{\partial\psi}{\partial\zeta} + \frac{1}{2}\nabla_{\perp}^2\psi - \theta\psi = -i\frac{\alpha}{2}\psi, \quad -\sigma^2\nabla_{\perp}^2\theta + \theta = |\psi|^2, \quad (1)$$

where $\psi = \sqrt{\chi L_d} E$ is the normalized field envelope ($I \equiv |E|^2$ is the intensity), $\theta = k_0 \Delta n L_d$, with Δn the nonlinear refractive index, $L_d = k_0 n_0 w_0^2$ the diffraction length, $\chi = k_0 n_2$, $k_0 = 2\pi/\lambda$, and n_0 the refractive index. $\alpha = \alpha_0 L_d$ is the normalized loss coefficient defined in terms of the power absorption coefficient α_0 . Transverse spatial coordinates are scaled as $\xi, \eta = x/w_0, y/w_0$, while $\zeta = z/L_d$. Here σ is the *degree of nonlocality*, used as a fitting parameter below. Figures 1a-c show three collected images of the transverse distribution of the beam intensity along z , for $w_0 = 25\mu\text{m}$ and three beam powers P in sample A. In Fig. 1a, corresponding to the lowest P , the beam shape does not change (diffraction is weak) along propagation and the shock does not occur. The presence of oscillatory SW can be observed in the other two images reported in Fig. 1b and Fig. 1c at higher powers, and in Figs. 1e-g where the 2-D profiles of the transmitted beam (on x - y plane) at the exit facet are reported. The x -profiles display post-shock rings that

increase in number and visibility with P , with outer rings being more intense than the inner ones, as typical for dispersive SW from Gaussian beams in nonlocal media. Figures 1d and 1h present beam propagation and transmission results obtained from simulations, performed by using input parameters identical to those in experiments and $\sigma = 0.2$. Shock occurs in the regime

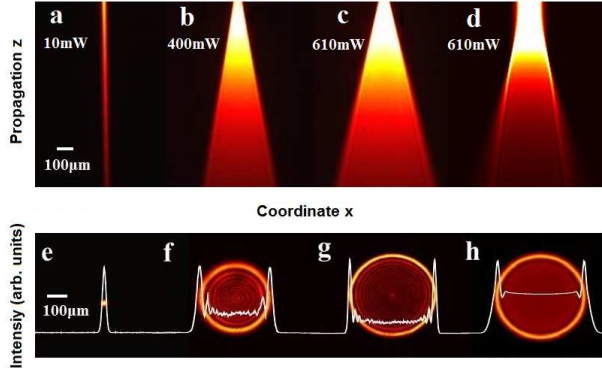


Fig. 1. (Color online) (a-d) Beam propagation as observed from top fluorescence emission for three different input powers (a-c) and calculated by numerical simulation (d); (e-g) corresponding transmitted intensity in the experiments and (h) in the simulations. Superimposed curves give the intensity x-profile.

$L_{nl} \ll L_\alpha, L_d$ [2–4], with $L_\alpha = 1/\alpha_0$ the absorption length, and $L_{nl} = 1/\chi I(x, 0)_{peak}$ is the nonlinear length (at the highest powers in our experiment, $L_{nl}/L_\alpha \sim 0.002$ and, in terms of the smallness parameter defined in Refs. [16, 17], $\varepsilon = \sqrt{L_{nl}/L_d} \sim 0.015$). This means that the involved length scales are such that the beam is mainly affected by the nonlinear defocusing effect rather than by absorption and diffraction. In this regime, as a first approximation, the beam phase depends on the intensity profile as $\phi(\xi, \eta, \zeta) = \frac{k_0 \zeta}{n_0} \Delta n(I(\xi, \eta))$. As discussed in Ref. [16], SW originates in correspondence with the chirp singularity $|d\phi/d\xi| \rightarrow \infty$ from which the shock distance can be analytically determined in the hydrodynamical approximation. For a generic degree of nonlocality and by assuming, for the sake of simplicity, a one-dimensional generic response function $K(\xi - \xi')$ yielding the index change as $\Delta n = \int d\xi' K(\xi - \xi') I(\xi', \eta)$ [Eqs. (1) imply a 2-D Lorentzian kernel K as one can easily verify by taking the Fourier transform of the second equation], we have:

$$\frac{\partial \phi}{\partial \xi} = \frac{k_0 \zeta}{n_0} \int d\xi' K(\xi - \xi') \frac{\partial I}{\partial \xi'}, \quad (2)$$

and the maximum of $\text{grad}(\phi)$ along z (or ζ) gives the shock position. Since K is z -independent the shock-point $z_s = \zeta L_d$ can be directly estimated both in experiments and simulations as the point of largest steepness of beam intensity, as detailed below. We note that in the highly nonlocal regime, $K(\xi) = K_0$, and correspondingly $\partial_\xi \phi = (k_0 \zeta K_0 / n_0) \int_\xi \partial_\xi I = 0$, i.e., as the de-

gree of nonlocality increases, the response function filters out all the edge frequencies in the broadened intensity spectrum in proximity of the shock-point, thus delaying it. In the highly nonlocal limit, the mean-field approximation fully smooths out all the singularities and the shock disappears. To estimate the point of shock formation both in experiments and simulations, we calculate the x -derivative $\partial_x I_N$ of the intensity normalized to its peak value, say $I_N(x, z)$. We define the steepness $S(z)$ as the maximum over x (at any z) of the derivative $S(z) = \max_x [\partial_x I_N(x, z)]$. Then the shock distance z_s is defined as the distance z corresponding to the maximum steepness, $[\max_z (S(z)) \rightarrow z = z_s]$. We follow this procedure for the whole set of images. In Fig. 2 we show representative profiles along with their derivatives at the input (Fig. 2a), right at the shock position (Fig. 2b), and beyond z_s (Fig. 2c), the steepness resulting the highest in Fig. 2b where the shock occurs. The behavior of the

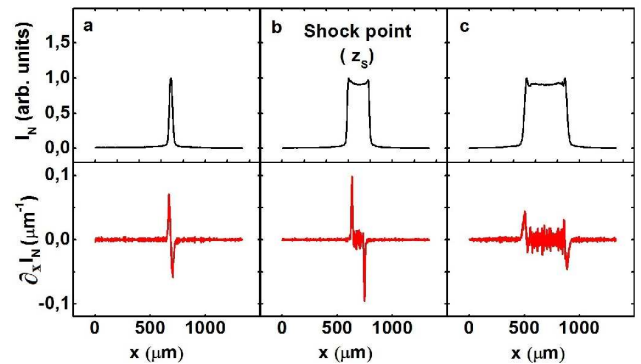


Fig. 2. (Color online) Normalized intensity profiles I_N (black line) along with derivative ($\partial_x I_N$, red line) for three different z at $P=600\text{mW}$: (a) input, $z = 0$; (b) $z = z_s = 273\mu\text{m}$, shock point; (c) $z = 850\mu\text{m}$, post-shock.

steepness S along z as obtained from experimental data is illustrated in Fig. 3 for three power values. The shock distance z_s is given by the position of the peak of the ten-degree polynomial fitting curve (solid curves through data). In Fig. 3 it is clear that this distance is shorter for increasing power, meaning that larger laser intensities speed up the shock formation process. We report in Fig. 4 the measured shock distance versus laser power, comparing with simulations. In particular Fig. 4a compares the shock point behavior for two beam waists in the same sample (B), whereas Fig. 4b compares the behavior in the two samples at a given beam waist ($25\mu\text{m}$). These data show quantitatively how both increasing input intensity or dye concentration speeds up shock formation because both result in a larger nonlinear response. In the simulations, we make use of the measured values of the physical parameters: $n_0 = 1.3$, $\alpha_0 = 900$ (A) and 600 (B) m^{-1} ; $\alpha_{NL} = 1.3 \times 10^{-5}$ (A) and 1.2×10^{-6} (B) $\text{m}^2 \text{W}^{-1}$; $n_2 = 4 \times 10^{-11}$ (A) and 2.7×10^{-11} (B) $\text{m}^2 \text{W}^{-1}$, while σ is used as a free fitting parameter. The best-fit of numerical simulations with the experi-

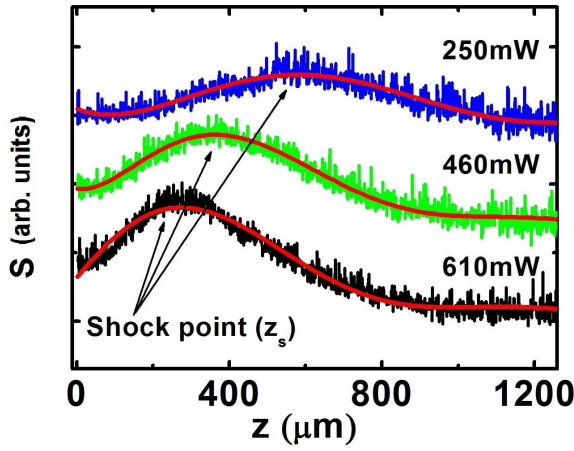


Fig. 3. (Color online) Steepness $S(z)$ of transverse profiles as function of z for three different powers. The point of maximum corresponds to shock distance z_s .

mental data in Fig. 4a, yields a degree of nonlocality $\sigma = 0.63$ ($w_0 = 18\mu\text{m}$) and 0.3 ($w_0 = 25\mu\text{m}$). Following Ref. [16], the nonlocality degree should scale with the inverse of beam waist. The observed slight discrepancy is attributed to the theoretical two-dimensional heat equation used to model the actual temperature profile in our sample. It is known from the hydrodynamic limit that the shock distance scales with power P according to the law $z_s \propto P^{-\gamma}$, with $\gamma = 0.5$ [16, 17]. This power law is confirmed by our experiments and simulations of Eqs. (1), though with deviations in the exponent. The experimental and numerical data given in Fig. 4, once fitted with γ as a free parameter, yield the following values: on sample A, $\gamma = 0.88$ ($w_0 = 25\mu\text{m}$), $\gamma = 1.0$ ($w_0 = 18\mu\text{m}$) and on sample B, $\gamma = 0.70$ ($w_0 = 25\mu\text{m}$), $\gamma = 0.72$ ($w_0 = 18\mu\text{m}$). The values of γ from the simulations are: on sample A, $\gamma = 0.43$ ($w_0 = 25\mu\text{m}$), on sample B: $\gamma = 0.57$ ($w_0 = 25\mu\text{m}$) and $\gamma = 0.43$ ($w_0 = 18\mu\text{m}$). The discrepancy between simulations and experiments is, once again, ascribed to the limits of validity of the 2D reduction of the heat equation adopted in Eqs. (1).

In conclusion, we use fluorescence imaging to directly monitor spatial wave-breaking. The full intensity distribution map allows us to experimentally determine the shock position for different nonlinearity and nonlocality. The comparison with numerical simulations of the non-local NLS model enables to quantify the limits of validity of the 2D reduction of the heat equation.

The research leading to these results has received funding from the European Research Council under the European Community's Seventh Framework Program (FP7/2007-2013)/ERC grant agreement n. 201766, from the Italian Ministry of Research (MIUR) through the PRIN project no.2009P3K72Z and from the Italian Ministry of Education, University and Research under the Basic Research Investigation Fund (FIRB/2008) program/CINECA grant code RBFR08M3P4 and RBFR08E7VA. We thank M. Deen

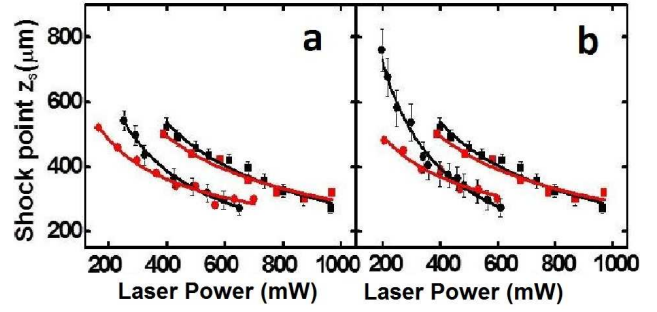


Fig. 4. (Color online) (a) Shock position z_s versus input power for sample B at two different beam waists: \blacksquare $25\mu\text{m}$, \bullet $18\mu\text{m}$; (b) Shock position vs. input power for beam waist $= 25\mu\text{m}$ and different dye concentrations: \blacksquare 0.067 mM , \bullet 0.1 mM . Experiments are denoted by black (dark) and simulations by red (clear) symbols.

Islam for the technical assistance.

References

1. G. B. Whitman, *Linear and Nonlinear Waves* (Wiley, New York, 1974).
2. A. Gurevich and L. P. Pitaevskii, *Sov. Phys. JETP* **38**, 291 (1973).
3. J. C. Bronski and D. McLaughlin, in *Singular Limits of Dispersive Waves* (Plenum, New York, 1994).
4. A. M. Kamchatnov, R. A. Kraenkel, and B. A. Umarov, *Phys. Rev. E* **66**, 036609 (2002).
5. R. J. Taylor, D. R. Baker, and H. Ikezi, *Phys. Rev. Lett.* **24**, 206 (1970).
6. J. E. Rothenberg and D. Grischkowsky, *Phys. Rev. Lett.* **62**, 531 (1989).
7. C. Conti, S. Stark, P. S. J. Russell, and F. Biancalana, *Phys. Rev. A* **82** (2010).
8. W. Wan, S. Jia, and J. Fleischer, *Nature Phys.* **3**, 46 (2007).
9. M. A. Hoefer, M. J. Ablowitz, I. Coddington, E. A. Cornell, P. Engels, and V. Schweikhard, *Phys. Rev. A* **74**, 023623 (2006).
10. A. M. Deykoon and G. A. Swartzlander, *J. Opt. Soc. Am. B* **18**, 804 (2001).
11. J. Wyller, W. Krolikowski, O. Bang, and J. J. Rasmussen, *Phys. Rev. E* **66**, 066615 (2002).
12. C. Conti, M. Peccianti, and G. Assanto, *Phys. Rev. Lett.* **92**, 113902 (2004).
13. G. A. Wurtz, R. Pollard, W. Hendren, G. P. Wiederrecht, D. J. Gosztola, V. A. Podolskiy, and A. V. Zayats, *Nat. nano.* **6**, 107 (2011).
14. C. Conti and E. DelRe, *Phys. Rev. Lett.* **105**, 118301 (2010).
15. C. Barsi, W. Wan, C. Sun, and J. W. Fleischer, *Opt. Lett.* **32**, 2930 (2007).
16. N. Ghofraniha, C. Conti, G. Ruocco, and S. Trillo, *Phys. Rev. Lett.* **99**, 043903 (2007).
17. C. Conti, A. Fratalocchi, M. Peccianti, G. Ruocco, and S. Trillo, *Phys. Rev. Lett.* **102**, 083902 (2009).
18. A. Minovich, D. N. Neshev, A. Dreischuh, W. Krolikowski, and Y. S. Kivshar, *Opt. Lett.* **32**, 1599 (2007).

References

1. G. B. Whitman, *Linear and Nonlinear Waves* (Wiley, New York, 1974).
2. A. Gurevich and L. P. Pitaevskii, *stationary structure of a collisionless shock wave*. Sov. Phys. JETP **38**, 291 (1973).
3. J. C. Bronski and D. McLaughlin, in *Singular Limits of Dispersive Waves* (Plenum, New York, 1994).
4. A. M. Kamchatnov, R. A. Kraenkel, and B. A. Umarov. *Asymptotic soliton train solutions of the defocusing nonlinear Schrödinger equation*. Phys. Rev. E **66**, 036609 (2002).
5. R. J. Taylor, D. R. Baker, and H. Ikezi. *Observation of Collisionless Electrostatic Shocks*. Phys. Rev. Lett. **24**, 206 (1970).
6. J. E. Rothenberg and D. Grischkowsky. *Observation of the Formation of an Optical Intensity Shock and Wave Breaking in the Nonlinear Propagation of Pulses in Optical Fibers*. Phys. Rev. Lett. **62**, 531 (1989).
7. C. Conti, S. Stark, P. S. J. Russell, and F. Biancalana. *Multiple hydrodynamical shocks induced by the Raman effect in photonic crystal fibers*. Phys. Rev. A **82**, 013838 (2010).
8. W. Wan, S. Jia, and J. Fleischer. *Dispersive superfluid-like shock waves in nonlinear optics*. Nature Phys. **3**, 46 (2007).
9. M. A. Hoefer, M. J. Ablowitz, I. Coddington, E. A. Cornell, P. Engels, and V. Schweikhard. *Dispersive and classical shock waves in Bose-Einstein condensates and gas dynamics*. Phys. Rev. A **74**, 023623 (2006).
10. A. M. Deykoon and G. A. Swartzlander. *Pinched optical-vortex soliton*. J. Opt. Soc. Am. B **18**, 804 (2001).
11. J. Wyller, W. Krolikowski, O. Bang, and J. J. Rasmussen, *Generic features of modulational instability in nonlocal Kerr media*. Phys. Rev. E **66**, 066615 (2002).
12. C. Conti, M. Peccianti, and G. Assanto. *Observation of Optical Spatial Solitons in a Highly Nonlocal Medium*. Phys. Rev. Lett. **92**, 113902 (2004).
13. G. A. Wurtz, R. Pollard, W. Hendren, G. P. Wiederrecht, D. J. Gosztola, V. A. Podolskiy, and A. V. Zayats. *Designed ultrafast optical nonlinearity in a plasmonic nanorod metamaterial enhanced by nonlocality*. Nat. nano. **6**, 107 (2011).
14. C. Conti and E. DelRe. *Optical Supercavitation in Soft Matter*. Phys. Rev. Lett. **105**, 118301 (2010).
15. C. Barsi, W. Wan, C. Sun, and J. W. Fleischer. *Dispersive shock waves with nonlocal nonlinearity*. Opt. Lett. **32**, 2930 (2007).
16. N. Ghofraniha, C. Conti, G. Ruocco, and S. Trillo. *Shocks in Nonlocal Media*. Phys. Rev. Lett. **99**, 043903 (2007).
17. C. Conti, A. Fratalocchi, M. Peccianti, G. Ruocco, and S. Trillo. *Observation of a Gradient Catastrophe Generating Solitons*. Phys. Rev. Lett. **102**, 083902 (2009).
18. A. Minovich, D. N. Neshev, A. Dreischuh, W. Krolikowski, and Y. S. Kivshar. *Experimental reconstruction of nonlocal response of thermal nonlinear optical media*. Opt. Lett. **32**, 1599 (2007).